IEEE Access
Multidisciplinary | Rapid Review | Open Access Journal

Received February 9, 2022, accepted February 19, 2022, date of publication February 24, 2022, date of current version March 9, 2022.

Digital Object Identifier 10.1109/ACCESS.2022.3154424

Balanced Heterodyne Brillouin Spectroscopy Towards Tissue Characterization

MELANIE SCHÜNEMANN[1,2], KARSTEN SPERLICH[1,2], KAI BARNSCHEIDT[3], SAMUEL SCHÖPA[3], JOHANNES WENZEL[4], STEFAN KALIES[4], ALEXANDER HEISTERKAMP[4], HEINRICH STOLZ[3], OLIVER STACHS[1,2], AND BORIS HAGE[2,3]

[1]Department of Ophthalmology, Rostock University Medical Center, 18057 Rostock, Germany
[2]Department Life, Light & Matter, University of Rostock, 18051 Rostock, Germany
[3]Institute of Physics, University of Rostock, 18051 Rostock, Germany
[4]Institute of Quantum Optics, Leibniz University Hannover, 30167 Hannover, Germany

Corresponding author: Melanie Schünemann (melanie.schuenemann@uni-rostock.de)

This work was supported by the Deutsche Forschungsgemeinschaft under Grant STA-543/9-1 and Grant HE 3644/7-1.

ABSTRACT We present the first application of balanced heterodyne detection, established in quantum optics, to Brillouin spectroscopy in biological tissues. The balanced detection cancels out a large part of the influence of the laser noise. The center wavelength is 1064 nm and the frequency resolution is 30 MHz. The frequency resolution and the accessible frequency range are only limited by the measurement time and the laser tuning range (30 GHz), respectively. In this way, we were able to measure the Brillouin shift in acetone, water, gummy bears, glass, and even porcine eye lenses.

INDEX TERMS Biomechanics, brillouin scattering, measurement techniques, optical mixing, spectroscopy.

I. INTRODUCTION

The analysis of scattered light provides a significant amount of information about the scattering medium. The scattered light contains different frequency components, depending on the underlying scattering process, e.g. Rayleigh scattering, *i.e.* elastic scattering on small particles, and Brillouin scattering, *i.e.* inelastic scattering on propagating sound waves. Rayleigh scattering results in a line around the excitation frequency, whereas Brillouin scattering comes with a frequency shift, depending on the speed of sound and refractive index of the investigated media, the scattering angle, and the frequency of the excitation [1].

Here, we are especially interested in the Brillouin scattering, as the frequency shift as well as the linewidth of the Brillouin scattered light relate to material properties as, e.g. bulk modulus and bulk viscosity and hence rheological properties of biological tissue as e.g. the eye, lens, cornea, or even cells [2]. The possibilities to investigate the Brillouin scattered signal vary from Brillouin spectroscopy, cf. e.g. [3], [4], to Brillouin microscopy, cf. e.g. [2], [5]–[7], and can be done for spontaneous, cf. e.g. [3], [4], and stimulated, cf. e.g. [7], [8], Brillouin scattering. Here, we are concerning the Brillouin spectroscopy for spontaneous Brillouin scattering, but the presented method can be extended to stimulated Brillouin scattering and also Brillouin microscopy.

There are two possible experimental approaches to determine the Brillouin scattered signal, optical filter methods [3], [4], [9]–[14] and optical mixing or beating methods [15]–[18]. The first kind spectrally decomposes the scattered light by using some elaborate and complex filter [4], [12]–[14], [19]–[21]. These methods suffer from a spectral ambiguity and limited resolution due to the limited Q value and difficulties in determining the absolute frequency of the Brillouin shift [15], [22]–[24]. The optical mixing or beating methods are technologies that are transferred from radio technology. These techniques come in handy when the signal frequency of interest is unknown or, as it is the case in Brillouin scattering, in a frequency regime (e.g. optical frequencies), *i.e.* THz $\pm$ GHz (optical carrier $\pm$ Brillouin shift), which is difficult to directly detect with, e.g. photodiodes. Here, the signal is mixed with a local oscillator (LO) creating a beat signal, which contains the signal of interest, in this case, the Brillouin shifted signal. This transfers the signal from THz $\pm$ GHz to the more easily accessible MHz regime, depending on the frequency difference of signal and LO. In contrast to the so far performed beating methods [15]–[18], [24]–[31], in the here presented method

The associate editor coordinating the review of this manuscript and approving it for publication was Jingang Jiang.

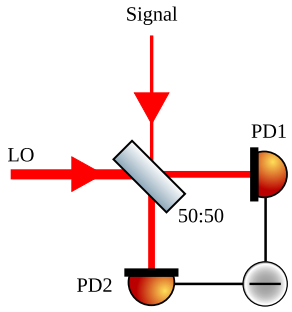

FIGURE 1. Schematic setup of the balanced heterodyne detection. The signal and the much stronger LO are overlapped on a 50:50 beam splitter and both output ports are detected with two photodiodes, PD1 and PD2, and the difference current of both detectors is the actual measurand.

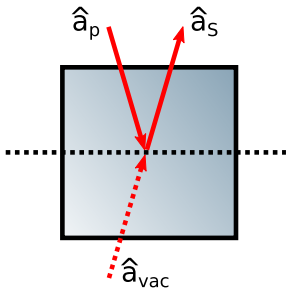

FIGURE 2. Schematic of the scattering process in the cuvette (top view). The pump mode entering the cuvette is denoted by $\hat{a}_P$. It is scattered on sound waves inside the sample resulting in the Brillouin scattered signal. Additionally, we have a vacuum mode entering the cuvette which is combined with the reflected pump and the Brillouin mode, resulting in the signal mode $\hat{a}_S$. This combination of both fields is equivalent to the combination of two modes on a beam splitter. The origin of the beam splitting reflectively, which is in general close to 0, is linked to the Brillouin scattering process and the signal mode is almost completely composed of the vacuum mode.

of balanced heterodyne Brillouin spectroscopy the signal and the LO interfere on a 50:50 beam splitter (BS), then both outputs of the BS are detected with photodiodes and the difference signal of both diodes is measured. This is a very common technology in radio frequency detection and quantum optics [32]–[41] and we apply it to Brillouin spectroscopy. By scanning the frequency of the LO, we are able to investigate a large frequency range and study the Brillouin shift of very different materials varying from acetone over water to porcine lenses, gummy bear (Haribo), and glass (SF10 glass, Schott AG, Germany), which are presented in the following.

II. GENERAL IDEA

This paper aims to transfer the well-established technology of balanced heterodyne detection to Brillouin spectroscopy. Balanced heterodyne detection is a mixing technique, where two laser beams (signal and LO), are overlapped on a 50:50 beam splitter and detected with two photodiodes, cf. Fig. 1. The difference of the currents measured with the two photodiodes is the measurand, which is further processed. In contrast to this, the so far published mixing or beating methods used in Brillouin spectroscopy, utilize only the signal of one photodiode. Here, the signal and LO are either overlapped in the probe, see e.g. [28]–[30] or a strong pump is sent into the probe creating the Brillouin scattered signal, which is then overlapped with the LO on a beam splitter afterward, see e.g. [24]–[26]. In the latter case, while working with only one photodiode it is possible to use a highly unbalanced beam splitter. This ensures that a large part of the signal is sent into the detection step and, as the LO power is usually not limited technically, it can be increased, ensuring that the LO is far stronger than the signal in the detection step. However, this implies that the noise of the laser influences the measurement directly.

The benefit of our presented method is, that we overlap the Brillouin scattered light with the LO on a 50:50 beam splitter and detect the outputs of both ports with photodetectors, cf. Fig. 1 and [42]. In this way, we are able to detect all of the Brillouin scattered signal, which is incident on the heterodyne beam splitter. Additionally, measuring the difference of both photodiodes in this balanced setup has the benefit that the LO noise from our measurement within the detection bandwidth is removed. The two modes incident on the 50:50 beam splitter are the LO $\hat{a}_{LO}$ and the signal field

$$\hat{a}_S = \sqrt{\rho_B}\hat{a}_B + (1 - \sqrt{\rho_B})\hat{a}_{vac}, \tag{1}$$

where ρ_B is the reflectance resulting from the scattering cross-section of the Brillouin scattering process and $\hat{a}_B$ and $\hat{a}_{vac}$ are the annihilation operators of the Brillouin scattered mode and vacuum mode, respectively. The signal mode $\hat{a}_S$ is created inside the sample or cuvette, cf. Fig. 2, via the Brillouin scattering inside the sample and an overlap of the scattered mode with a vacuum mode. This overlap is similar to the overlap of two modes on a beam splitter. Note, that a priori knowledge of ρ_B, and hence of the scattering cross-section σ_B, is not necessary in the detection process. Moreover, it is in principle possible to extract the absolute value of σ_B from the measured Brillouin signal after the measurement, through a direct reference of the signal to the vacuum noise. The output fields of the beam splitter, which are incident on the two photodetectors, read as

$$\hat{a}_{PD1/PD2} = \frac{1}{\sqrt{2}}\left(\hat{a}_{LO} \pm \hat{a}_S\right) \tag{2}$$

respectively, cf. [42]. The sign difference between the output fields results from the energy conservation which reflects one possible phase relation between the two input fields. The resulting difference current is

$$I_{Diff} \propto \left|\hat{a}_{PD1}\right|^2 - \left|\hat{a}_{PD2}\right|^2 \tag{3}$$

$$= \hat{a}_S^\dagger \hat{a}_{LO} + \hat{a}_{LO}^\dagger \hat{a}_S. \tag{4}$$

Using

$$\hat{a}_n = \left(\alpha_n + \delta\hat{a}_n\right)\exp(\mathrm{i}\omega_n t) \tag{5}$$

$$\hat{a}_n^\dagger = \left(\alpha_n^* + \delta\hat{a}_n^\dagger\right)\exp(-\mathrm{i}\omega_n t), \tag{6}$$

where $n = \mathrm{LO}, \mathrm{B}, \mathrm{vac}$ (LO mode, Brillouin mode, and vacuum mode, respectively). α_n are the coherent amplitudes, ω_n are the angular frequencies, and $\delta\hat{a}_n$ and $\delta\hat{a}_n^\dagger$ are the field fluctuations. Additionally, we only consider terms linear in the coherent amplitude of the LO α_{LO} and linear in the fluctuations of the Brillouin scattered ($\delta\hat{a}_{\mathrm{B}}$ and $\delta\hat{a}_{\mathrm{B}}^\dagger$) and vacuum mode ($\delta\hat{a}_{\mathrm{vac}}$ and $\delta\hat{a}_{\mathrm{vac}}^\dagger$). This is reasonable as the coherent amplitudes of the Brillouin scattered and the vacuum mode are much smaller than the amplitude of the LO, and hence, they do not contribute to the signal. Therefore, we obtain the difference current

$$I_{\mathrm{Diff}} \approx \alpha_{\mathrm{LO}} \left(\sqrt{\rho_{\mathrm{B}}}\delta\hat{a}_{\mathrm{B}}^\dagger \exp(\mathrm{i}(\omega_{\mathrm{LO}} - \omega_{\mathrm{B}})t) + (1 - \sqrt{\rho_{\mathrm{B}}})\delta\hat{a}_{\mathrm{vac}}^\dagger \exp(\mathrm{i}(\omega_{\mathrm{LO}} - \omega_{\mathrm{vac}})t) \right) + h.c. \quad (7)$$

Hence, the detected difference current scales with the coherent amplitude of the LO and contains the fluctuations of the Brillouin scattered and vacuum mode. The frequency of the Brillouin scattered signal is given by the Brillouin shift specific to the sample and the incident pump frequency, and hence, is fixed. The beating frequency of interest is $\Delta\omega = \omega_{\mathrm{LO}} - \omega_{\mathrm{B}}$. The detectors used measure only the difference current with a specific bandwidth BW around $\Delta\omega$. As BW is approximately 30 MHz, only a part of the spectrum is detected by looking at one $\Delta\omega$. Therefore, the frequency of the LO is varied in order to scan a larger frequency range, and with that, the full Brillouin peak. The frequency of the vacuum mode actually uniformly stretches over the whole spectrum, hence, the contribution of the vacuum mode to the final signal is the same for all difference frequencies $\omega_{\mathrm{LO}} - \omega_{\mathrm{vac}}$. Due to the limited BW, only frequency components of the vacuum similar to ω_{B} are detected.

III. EXPERIMENTAL SETUP

The experimental setup contains two lasers as main laser and LO laser (Innolight Diabolo (linewidth ≈1 kHz over 100 ms) and Coherent Mephisto S (linewidth <1 kHz over 100 ms), respectively), both operating around 1064 nm with a frequency stability of 2 MHz/min. Moreover, the Mephisto S has a 30 GHz tuning range. This tuning range, which is achieved by applying a voltage onto the laser crystal changing the crystal temperature, is used to vary the beating frequency in the balanced heterodyne detector in order to obtain the Brillouin spectrum. Please note, that the general method is not limited to the wavelength of 1064 nm, but can be applied for any arbitrary wavelength, and hence, the optimal wavelength in regard of the Brillouin shift and Brillouin gain for a specific probe can be used. Furthermore, if the probe is sensible to phototoxicity or a specific imaging depth is necessary, this can also be taken into account for the used wavelength. It was chosen here however, as the two used laser sources and the photo diodes were available in the laboratory. Both lasers are split into two beams with a half-waveplate and a polarizing beam splitter (PBS). This results in adjustable splitting ratios, and hence, the laser power in each beam can be changed during the experiment if needed. Note that more combinations of half-waveplate and PBS are used in the setup to optimize the laser power and polarization throughout the experiment. However, for the sake of simplicity, they are not shown in Fig. 3. One beam of each laser is used to overlap both lasers on a fast photodiode (beat note diode in Fig. 3, Thorlabs GmbH DET08C/M), specified for measuring

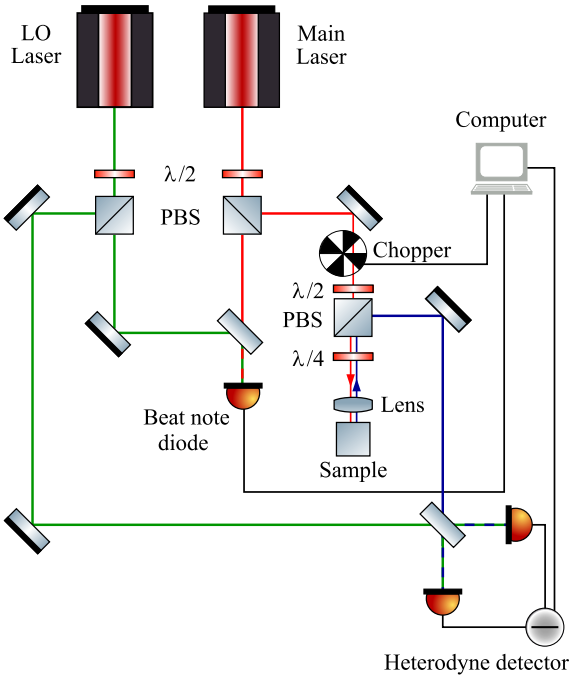

FIGURE 3. Schematic of the experimentally realized setup. The two lasers (Innolight Diabolo and Coherent Mephisto S) are overlapped on a fast photodiode (beat note diode) to measure the beat frequency between the two lasers. The main laser (red) is sent through a chopper, periodically blocking the signal, and is afterwards focused into the sample. The Brillouin backscattered light (blue) is sent into the heterodyne detector, where it is overlapped on a 50:50 beam splitter with the local oscillator (green). The AC signals of the photodiodes are subtracted and sent to the computer, where the difference signal is further processed, along with the signal from the GHz diode and a trigger signal from the chopper.

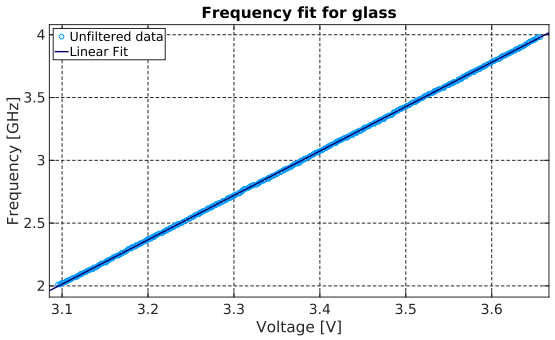

FIGURE 4. Determined beating frequency from 2 GHz to 4 GHz detected during the measurement of glass (SF10) dependent on the voltage applied to the laser crystal of the Mephisto S laser (blue circles). The linear fit ($f(V) = a \cdot V + f_0$, with $a = (3.5330 \pm 0.0028)$ GHz/V and $f_0 = (-8.938 \pm 0.009)$ GHz), enables us to determine the beating frequency above 5 GHz. Note, the fit has a linear correlation coefficient of $R^2 = 0.9999$.

frequencies up to 5 GHz. The determination of the beat frequency from 10 MHz to 5 GHz is done with an oscilloscope (Rohde & Schwarz RTO 1024) and sent to a computer, cf. Fig. 4. Fig. 4 shows the determined beating frequency from 2 GHz to 4 GHz detected during the measurement of glass (SF10) depending on the voltage applied to the laser crystal of the Mephisto S. This applied voltage changes the crystal temperature, and hence, the laser frequency of the Mephisto S, and therefore, the beating frequency. The resulting linear fit ($f(V) = a \cdot V + f_0$, with $a = (3.5330 \pm 0.0028)$ GHz/V and $f_0 = (-8.938 \pm 0.009)$ GHz), with a linear correlation coefficient of $R^2 = 0.9999$, is used to determine the beat frequency above 5 GHz. To ensure, that this frequency estimation reflects the actual beating frequency, we start the measurement in a regime in which the fast photodiode still reliably detects the beating frequency, as the exact voltage dependence of the frequency changes due to the temperature and humidity of the laboratory. The main laser is focused into the sample acting as the probe for the Brillouin scattering. The incoming beam has a power of approximately 72 mW with a beam waist (radius) of 0.277 mm in front of the focusing lens corresponding to an average intensity of 0.299 MW/m^2. The focusing lens is an objective lens with a focal length of 5.8 mm, a magnification of 20 and, a numerical aperture of 0.35, resulting in a focus waist (radius) of 7.1 μ m and a Rayleigh range of 148 μ m in air. For the values in the medium, these values must be multiplied by the corresponding refractive index of the medium. Neglecting any losses, the intensity in the focused spot in air is 455 MW/m^2. Note that the intensity in the medium scales with $1/n^2$, since the focus waist depends linearly and consequently the focus area quadratically on the refractive index. The power in the signal beam ($\approx$ 50 μ W) originates almost entirely from Fresnel reflection on optical surfaces in the beam path. Before entering the sample, the beam passes a chopper, periodically blocking and unblocking the incoming laser beam with a frequency of 20 Hz. In this way, we reference the measured variance with an open chopper to the measured variance with a closed chopper during the measurement, ensuring that slow laser power fluctuations are not affecting the result. The quarter-waveplate between PBS and sample is used to rotate the polarization of the incoming and reflected beam to deflect the backscattered light with the PBS to the heterodyne detector. Here, care was taken to avoid the direct reflex from the sample surface, e.g. a cuvette, entering the heterodyne detector, as this would mask any Brillouin scattered signal. This is done by aligning the direct reflex from the sample surface in a way, that it is not back-reflected into the PBS, and hence, not reflected into the heterodyne detector. This is reasonable, for two different reasons. First, we avoid the direct reflex from the sample surface, since it contains a much higher percentage of Rayleigh signal and lower percentage of Brillouin signal, simply due to the higher amount of reflected light based on the refractive index change from air to sample. Therefore, the detectors would be saturated without being able to detect the weak Brillouin signal. Second, without the direct reflection from the sample or cuvette surface, the ratio of Rayleigh to Brillouin signal is lower and it is in fact even possible to also measure the Rayleigh scattered peak. However, as this signal is still much stronger than the Brillouin signal, we would have to reduce the signal power before sending it into the heterodyne detector, as we would otherwise overpower the photodiodes, too. This would decrease the signal-to-noise ratio of the Brillouin peaks. The LO laser entering the heterodyne detector has a power of 1.2 mW. The LO and the Brillouin scattered light are superimposed on a 50:50 beam splitter and afterwards detected by two photodiodes. Each detecor consists of a FD300S3 photodiodes from Fermionics Opto-Technology, USA, and a self-designed and self-made amplifyer. They are matched and optimized in order to achieve almost identical detectors regarding quantum efficiency, transfer functions and spectra. At this LO power level, the photodiodes have a dark noise clearance of more than 10 dB. The difference signal of the two photodiodes is the measurand. In order to obtain one Brillouin spectrum, the frequency of the LO laser is scanned over a probe specific frequency range, by changing the laser crystal temperature (−3 GHz/K), in a set number of data points, here usually 1000. The frequency scan is done from the start frequency (f_0) to a maximum frequency (f_m) and back to the start frequency. This scan must be slow enough to ensure, that the frequency is stable for each measurement point. For each measurement point data is averaged over 50 ms, which improves the signal-to-noise ratio, where the noise here is the vacuum noise. Due to post measurement data selection, where 500 data points are selected, for a scan from f_0 to f_m, the measurement time for a single scan is approximately 0.5 min. This is later referred to as single measurement.

IV. RESULTS AND DISCUSSION

Figures 5 to 8 show the first successful measurements of the Brillouin shift using our presented method of balanced heterodyne Brillouin spectroscopy. The presented data are gained in either a single measurement (acetone) or averaged over a number of single measurements, in the case of water over 5, the pig lens over 10, gummy bear over 180, and glass over 180 measurements. The data shown in Fig. 5 are only the unfiltered data, whereas in Figs. 6 to 8 the unfiltered data along with data filtered by a moving mean over a window of 12 neighboring data points is shown for better visualization. The fit in each figure, which is done with the unfiltered data, is a Lorentzian fit of the form

$$L(\nu) = \frac{a}{1 + 4\frac{(\nu - \nu_B)^2}{\Delta\nu_B^2}} + c, \tag{8}$$

where a corresponds to the height of the function, ν_B is the Brillouin frequency shift, $\Delta\nu_B$ is the Brillouin linewidth, and c is an offset, which results from the non-vanishing power in the signal port. Note, that for the sake of simplicity a Lorentzian fit is used here instead of a Voigt profile. A direct comparison of the absolute values of the height of the fit function is not possible, as it depends on the reflectance

TABLE 1. Experimentally determined Brillouin shift $\nu_{B,E}$ and linewidth $\Delta\nu_{B,E}$ according to Eq. (8) measured in backscattering geometry and 1064 nm central wavelength and the respective literature values, $\nu_{B,L}$ and $\Delta\nu_{B,L}$, for acetone and water [43] and SF10 [45]. The given errors for the experimentally measured values result from the 95% confidence interval of the specific fit. Note, that if the beating frequency exceeds 5 GHz (here Porcine lens, Gummy bear and SF10), and hence, is gained through the linear fit, the relative error resulting from the 95% confidence interval of the linear fit, is also included in the given errors through linear error propagation. † *Ranging from 4.0 GHz to 4.7 GHz for capsular and central region, respectively [19].* * *Data points were taken from the respective graph in [45] and the Brillouin shift was obtained from a fit according to Eq.* (8) *and corrected for backscattering geometry, 1064 nm and refractive index. Due to the poor spectral resolution in [45] no reasonable linewidth could be obtained.*

Material	$\nu_{B,E}$/ GHz	$\Delta\nu_{B,E}$/ MHz	$\nu_{B,L}$/ GHz	$\Delta\nu_{B,L}$/ MHz
Acetone	2.9982±0.0015	101±5	2.97-3.1	90-119
Water	3.702±0.004	153±12	3.7	152
Porcine lens	4.70±0.06	726±230	4.0-4.7 GHz†	
Gummy bear	9.16±0.09	663±200		
SF10	12.937±0.027	45±7	13.059±0.0013 *	*

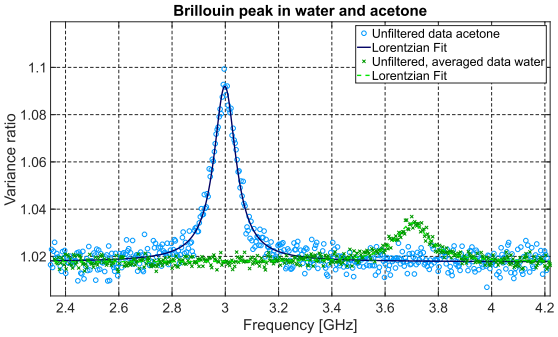

FIGURE 5. Measured Brillouin spectrum in acetone (data in blue o's, Lorentzian fit as blue solid line) obtained in a one-shot measurement of approximately 0.5 minute and in water (data in green x's, Lorentzian fit as green dashed line) obtained by averaging over five single measurements of approximately 2.5 minutes and a total measurement time of five minutes. The Lorentzian fits give $\nu_B = (2.9982 \pm 0.0015)$ GHz and $\Delta\nu_B = (101 \pm 5)$ MHz while an overall relative error of 6 % for the spectrum (see text) of acetone and $\nu_B = (3.702 \pm 0.004)$ GHz and $\Delta\nu_B = (153 \pm 12)$ MHz with an overall relative error of 10 % for the spectrum water.

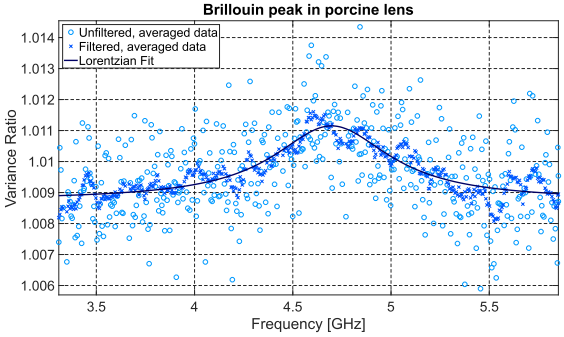

FIGURE 6. Measured Brillouin peak in an *ex vivo* porcine lens obtained by averaging over ten single measurements of approximately 5 minutes and a total measurement time of ten minutes. The unfiltered data is shown in light blue o's and the data filtered with a moving mean over 12 neighboring data points is shown in dark blue x's. The Lorentzian fit gives $\nu_{B,Lens} = (4.70 \pm 0.06)$ GHz and $\Delta\nu_{B,Lens} = (726 \pm 230)$ MHz while the overall relative error of the spectrum of the porcine lens is 34 %.

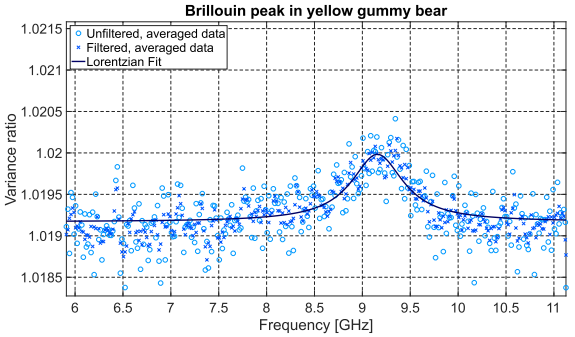

FIGURE 7. Measured Brillouin peak in a yellow gummy bear (Haribo) by averaging over 180 single measurements of approximately 90 minutes and a total measurement time of 180 minutes. The unfiltered data is shown in light blue o's and the data filtered with a moving mean over 12 neighboring data points is shown in dark blue x's. The Lorentzian fit gives $\nu_{B,GB} = (9.16 \pm 0.09)$ GHz and $\nu_{B,GB} = (663 \pm 200)$ MHz while the overall relative error of the spectrum of the gummy bear is 35 %.

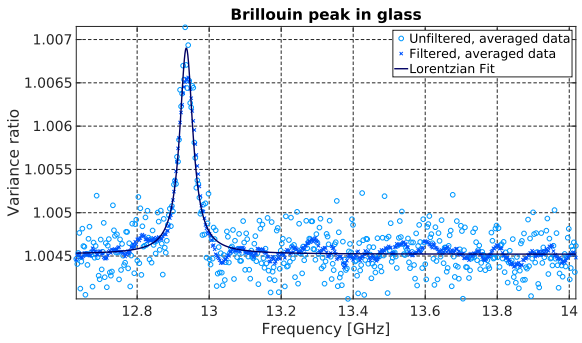

FIGURE 8. Measured Brillouin peak in glass (SF10, Schott AG) by averaging over 180 single measurements of approximately 90 minutes and a total measurement time of 180 minutes. The unfiltered data is shown in light blue o's and the data filtered with a moving mean over 12 neighboring data points is shown in dark blue x's. The Lorentzian fit gives $\nu_{B,SF10} = (12.937 \pm 0.027)$ GHz and $\Delta\nu_{B,SF10} = (45 \pm 7)$ MHz while the overall relative error of the spectrum of SF10 is 20 %.

ρ_B (in Eq. (1)), the Brillouin gain of the investigated material, and the losses in the balanced heterodyne detector, e.g. the non-unity visibility which varies from measurement to measurement. Hence, these fits give information about the Brillouin shift and linewidth of the investigated material. Moreover, we use the obtained fit parameter along with the corresponding 95 % confidence interval values in quadratic error propagation, in order to obtain an overall error for the measurement as a measure for the quality of our measured spectrum. For acetone and water, the Brillouin shifts for the respective wavelength are published. The presented results for the Brillouin shifts and linewidths in acetone and water are in good agreement with the literature [43], cf. Table 1.

The overall error of the spectrum of acetone is 6 % and of water 10 %. The measured values for acetone and water lie within the range of accepted values given in [43]. Small differences may arise in the temperature dependence of the refractive index and the speed of sound, and hence the temperature dependence of the Brillouin shift and linewidth, in the specific material. This is particularly relevant since we do not know the sample temperature precisely, although we monitor the laboratory temperature in the vicinity of the sample (21.5±0.5) °C and the literature values for the Brillouin shift and linewidth are given for an unspecified temperature. Furthermore, the detection bandwidth influences the measured linewidth, if the bandwidth is not significantly smaller than the Brillouin linewidth, which is not the case here. Our presented results are not corrected in terms of the detection bandwidth. In the case of the literature values, it is not clear what the detection bandwidth is and if the values are corrected in terms of the bandwidth or not. Conclusively, the measurements in acetone and water validate our heterodyne method, which we further extended to other materials beyond liquids such as soft materials, e.g. porcine lenses and gummy bears, and solids, e.g. glass.

Fig. 6 shows the *ex vivo* measured Brillouin spectrum of an enucleated porcine eye lens. The lens was placed inside a cuvette containing 0.9% sodium chloride solution. As the cuvette was not moved during the measurement, a movement of the porcine lens can be excluded. The data presented in Fig. 6 were averaged over 10 measurements, which corresponds to approximately 5 minutes within a total measurement time of approximately 10 minutes. The fit is performed with Eq. (8), too. The overall error of the spectrum of the porcine lens is 34 %. The measured Brillouin shift is $\nu_{\mathrm{B,Lens}} = (4.70 \pm 0.06)\,\mathrm{GHz}$ and the Brillouin linewidth is $\Delta\nu_{\mathrm{B,Lens}} = (726 \pm 230)\,\mathrm{MHz}$. Note that, due to the low power of the Brillouin signal, the fluctuations of the spurious signal power due to parasitic interferences have a stronger influence here than in the measurement of acetone or water, resulting in additional peaks on both sides of the Brillouin peak. In order to achieve a comparable signal-to-noise ratio for the porcine lens as for acetone, an averaging over more measurements is necessary. Nevertheless, this result demonstrates the capability of our method to investigate biological material. However, as the laser power, which is sent into the porcine lens is approximately 72 mW, this technique is not yet suitable for *in vivo* measurements. Nonetheless, this first detection of a Brillouin shift obtained by balanced heterodyne Brillouin spectroscopy in an eye lens of a vertebrate is already a promising result for further research for a possible application of this method in ophthalmology, e.g. the investigation of accommodation or diseases. The investigation of accommodation will support the search for suitable lens refilling materials potentially restoring accommodation [44]. Moreover, the here obtained results are comparable to the results obtained in [19]. There, Brillouin scattering in a porcine eye lens was measured with a laser beam at 780 nm in dependence of the focus position inside the lens and the time after extraction showing the post mortem tissue change. Even as the used wavelength differs in this measurement from ours, the results are still comparable, as the frequency shift scales with the wavelength. According to [19], the Brillouin shift in the center of the lens is approximately 6.4 GHz and 5.45 GHz in the capsular region for 780 nm. Rescaling it to 1064 nm results in a shift of 4.7 GHz in the center of the lens and about 4.0 GHz in the capsular region. This indicates that we measured in or near the center of the lens, as our measured Brillouin shift is (4.70±0.06) GHz. However, the exact Brillouin shift in the porcine eye lens depends not only on the focus position of the probe laser inside the lens but also on the post mortem delay, as the tissue changes rapidly. The time period after extraction in the here presented measurements is not precisely known, approximately 1-1.5 days, and hence, an exact comparison to the results obtained in [19] is difficult. Nevertheless, the presented Brillouin shifts in the post mortem porcine lens still resemble the results in [19]. Furthermore, even though the exact time after enucleation is unknown, we were also able to observe some post mortem tissue changes with our setup. As the post mortem time remains unknown and the aim of this work is to present and verify this method, these data are not presented here.

Figure 7 shows the Brillouin peak of a yellow gummy bear obtained by our method. The measured Brillouin shift is $\nu_{\mathrm{B,GB}} = (9.16 \pm 0.09)\,\mathrm{GHz}$ and the Brillouin linewidth is $\nu_{\mathrm{B,GB}} = (663 \pm 200)\,\mathrm{MHz}$ and the overall error of the spectrum of the gummy bear is 35 %. These values are calculated by the fit according to Eq. (8) using data averaged over 180 single measurements, which corresponds to approximately 90 minutes averaging time within a total measurement time of 3 hours. We are not aware of literature values for the Brillouin shift or linewidth of gummy bears as well as values for the refractive index or the speed of sound in a gummy bear. However, this result further confirms the power of our method, as we are not restricted to specific materials, but rather can investigate seemingly random materials. Moreover, this was a further extension to a detected beat frequency of up to 11 GHz. The long averaging time of almost three hours results from the strong absorption in the gummy bear, and as the signal is rather small, also probably from a small Brillouin gain.

Figure 8 shows the Brillouin peak of a SF10 glass obtained by our method. This measurement demonstrates the large accessible frequency range of the presented method. The estimated Brillouin shift is $\nu_{\mathrm{B,SF10}} = (12.937 \pm 0.027)\,\mathrm{GHz}$ and the Brillouin linewidth is $\Delta\nu_{\mathrm{B,SF10}} = (45 \pm 7)\,\mathrm{MHz}$. These values are calculated through the fit according to Eq. (8) using data averaged over 180 single measurements, which corresponds to approximately 90 minutes averaging time within 180 minutes total measurement time with an overall error of 20 %. A Brillouin spectrum for SF10 glass can be found in [45]. Note, that the authors used a different laser wavelength, $\lambda_{\mathrm{L}} = 514.5\,\mathrm{nm}$ instead of $\lambda_{\mathrm{L}} = 1064\,\mathrm{nm}$, and a different scattering angle, $\theta = 90°$ instead of $\theta = 180°$. However, as the Brillouin shift of

a medium can be calculated with the knowledge of the velocity of sound v_s, the refractive index of the medium n for the used laser wavelength λ_L and the scattering angle θ

$$\nu_B = \pm \frac{2\, v_s}{\lambda_L} \cdot n \cdot \sin(\theta/2)\,, \tag{9}$$

it is also possible to correct a given Brillouin shift for another setup if the laser wavelength, refractive index and scattering angle of both setups are known. We extracted data points from the Brillouin spectrum in [45], applied the fit according to Eq. (8) and corrected it to our setup. With this procedure the expected Brillouin shift could be determined to $\nu_{B,Lit} = 13.059 \pm 0.013$ GHz. The discrepancy between the literature and our measured value is only about 0.1 GHz. Considering that no exact temperature was specified in [45] and that no systematic errors were considered, these values are in good agreement.

The results of the yellow gummy bear and the SF10 glass emphasize the potential of our method, as we were able to extend the estimated frequency range to beating frequencies of approximately 13 GHz, which can be extended to 30 GHz with the presented method and is much higher than the limit of 3.6 GHz beating frequency detected in other beating methods [24]. It is worth noticing, that long measurement times are problematic in the investigation of living tissues. With our setup, we were able to reduce the measurement time in comparison to other beating methods. In the case of toluene, the measurement took around one hour [25], which has a Brillouin gain comparable to acetone (cf. [43]), measured in half a minute with our method. For optical filter methods measurement times for the Brillouin shift in biological tissue as low as 0.3 s were reported [19]. However, a direct comparison is difficult due to missing data of the signal-to-noise ratio or other comparable measures. Nevertheless, as the here presented results are the first proof of principle measurements, there is still room for improvement in terms of the measurement time, as this strongly depends on the investigated material, the optical quality of the setup, the laser stability, number of sampling points, and the bandwidth of the photodiodes, which will be further improved in future experiments.

V. SUMMARY AND CONCLUSION

We present the first application of balanced heterodyne detection, a method known from e.g. quantum optics, in Brillouin spectroscopy. Here, we overlap the weak Brillouin signal on a 50:50 beam splitter with a strong LO, enabling us to detect all of the Brillouin scattered signal, which is incident on the heterodyne beam splitter. The output of both beam splitter ports is detected with two photodiodes and the difference current of these photodiodes is the measurand. By measuring the difference of both photodiodes in this balanced setup the LO noise from our measurement within the detection bandwidth is removed. We present the quantum physical description of the balanced heterodyne Brillouin spectroscopy and its application in the experiment. The Brillouin peak of different materials including liquids (acetone and water), solids (glass), soft materials (gummy bears), and even biological tissues (porcine eye lenses) were successfully measured with our method. The results obtained for acetone and water validate our method, as we can reproduce the literature values for these samples. In comparison with other beating methods [15]–[18], we were able to extend the detectable beating frequency to 30 GHz, here shown up to 13 GHZ, and reduce the measurement time. The resolution of our measurement is limited by the detection bandwidth, and hence, the averaging time necessary to receive a Brillouin spectrum. Furthermore, the direct reference of our signal to the vacuum noise principally allows the estimation of the absolute value of the Brillouin scattering cross-section, however, in order to achieve this estimation, the overall quantum efficiency of the setup must be quantified.

REFERENCES

[1] M. Fox, *Optical Properties of Solids*, 2nd ed. London, U.K.: Oxford Univ. Press, 2010, pp. 289–290.
[2] G. Antonacci and S. Braakman, "Biomechanics of subcellular structures by non-invasive Brillouin microscopy," *Sci. Rep.*, vol. 6, no. 1, Dec. 2016, Art. no. 37217.
[3] R. Y. Chiao and B. P. Stoicheff, "Brillouin scattering in liquids excited by the He–Ne maser," *J. Opt. Soc. Amer.*, vol. 54, no. 10, p. 1286, Oct. 1964.
[4] D. H. Rank, E. M. Kiess, and U. Fink, "Brillouin spectra of viscous liquids," *J. Opt. Soc. Amer.*, vol. 56, pp. 163–166, Feb. 1966.
[5] R. Prevedel, A. Diz-Muñoz, G. Ruocco, and G. Antonacci, "Brillouin microscopy: An emerging tool for mechanobiology," *Nature Methods*, vol. 16, no. 10, pp. 969–977, Oct. 2019.
[6] Y. S. Ambekar, M. Singh, G. Scarcelli, E. M. Rueda, B. M. Hall, R. A. Poché, and K. V. Larin, "Characterization of retinal biomechanical properties using Brillouin microscopy," *J. Biomed. Opt.*, vol. 25, no. 9, pp. 1–7, Sep. 2020.
[7] I. Remer, R. Shaashoua, N. Shemesh, A. Ben-Zvi, and A. Bilenca, "High-sensitivity and high-specificity biomechanical imaging by stimulated Brillouin scattering microscopy," *Nature Methods*, vol. 17, no. 9, pp. 913–916, Sep. 2020.
[8] M. Damzen, V. Vlad, A. Mocofanescu, and V. Babin, *Stimulated Brillouin Scattering: Fundamentals and Applications*. Bristol, U.K.: IOP Publishing, 2003.
[9] G. B. Benedek, J. B. Lastovka, K. Fritsch, and T. Greytak, "Brillouin scattering in liquids and solids using low-power lasers," *J. Opt. Soc. Amer.*, vol. 54, no. 10, pp. 1284–1285, 1964.
[10] D. H. Rank, E. M. Kiess, U. Fink, and T. A. Wiggins, "Brillouin spectra of liquids using He–Ne laser," *J. Opt. Soc. Amer.*, vol. 55, no. 8, pp. 925–927, Aug. 1965.
[11] P. A. Fleury and R. Y. Chiao, "Dispersion of hypersonic waves in liquids," *J. Acoust. Soc. Amer.*, vol. 39, no. 4, pp. 751–752, Apr. 1966.
[12] J. Stone, "Hypersonic velocity measurements in aqueous alkali halide solutions," *J. Opt. Soc. Amer.*, vol. 56, no. 8, pp. 1136–1137, Aug. 1966.
[13] R. Vacher, H. Sussner, and M. V. Schickfus, "A fully stabilized Brillouin spectrometer with high contrast and high resolution," *Rev. Sci. Instrum.*, vol. 51, no. 3, pp. 288–291, Mar. 1980.
[14] R. Vialla, B. Rufflé, G. Guimbretière, and R. Vacher, "Eliminating the broadening by finite aperture in Brillouin spectroscopy," *Rev. Sci. Instrum.*, vol. 82, no. 11, Nov. 2011, Art. no. 113110.
[15] A. T. Forrester, R. A. Gudmundsen, and P. O. Johnson, "Photoelectric mixing of incoherent light," *Phys. Rev.*, vol. 99, no. 6, pp. 1691–1700, Sep. 1955.
[16] T. Yogi, K. Sakai, and K. Takagi, "Light beating spectroscopy of Brillouin scattering in gases and solids," *J. Appl. Phys.*, vol. 100, no. 2, Jul. 2006, Art. no. 023505.
[17] T. Matsuoka, K. Sakai, and K. Takagi, "Hyper-resolution Brillouin–Rayleigh spectroscopy with an optical beating technique," *Rev. Sci. Instrum.*, vol. 64, no. 8, pp. 2136–2139, Aug. 1993.

[18] H. Tanaka, T. Sonehara, and S. Takagi, "A new phase-coherent light scattering method: First observation of complex Brillouin spectra," *Phys. Rev. Lett.*, vol. 79, no. 5, pp. 881–884, Aug. 1997.
[19] S. Reiß, G. Burau, O. Stachs, R. Guthoff, and H. Stolz, "Spatially resolved Brillouin spectroscopy to determine the rheological properties of the eye lens," *Biomed. Opt. Exp.*, vol. 2, no. 8, pp. 2144–2159, 2011.
[20] S. Reiß, K. Sperlich, M. Hovakimyan, P. Martius, R. F. Guthoff, H. Stolz, and O. Stachs, "*Ex vivo* measurement of postmortem tissue changes in the crystalline lens by Brillouin spectroscopy and confocal reflectance microscopy," *IEEE Trans. Biomed. Eng.*, vol. 59, no. 8, pp. 2348–2354, Aug. 2012.
[21] O. Stachs, S. Reiß, R. Guthoff, and H. Stolz, "Spatially resolved Brillouin spectroscopy for *in vivo* determination of the biomechanical properties of the crystalline lenses," *Proc. SPIE*, vol. 8209, Mar. 2012, Art. no. 82090T.
[22] M. Balkanski, *Proceedings of the Second International Conference on Light Scattering in Solids*. Paris, France: Flammarion Sciences, Jul. 1971.
[23] J. M. Vaughan, *Photon Correlation and Light Beating Spectroscopy*, H. Z. Cummings and E. R. Pike, Eds. New York, NY, USA: Plenum, 1974, p. 429.
[24] H. Tanaka and T. Sonehara, "New method of superheterodyne light beating spectroscopy for Brillouin scattering using frequency-tunable lasers," *Phys. Rev. Lett.*, vol. 74, no. 9, pp. 1609–1612, Feb. 1995.
[25] H. Tanaka and T. Sonehara, "Superheterodyne light beating spectroscopy for Rayleigh–Brillouin scattering using frequency-tunable lasers," *Rev. Sci. Instrum.*, vol. 73, no. 5, pp. 1998–2010, May 2002.
[26] T. Sonehara and H. Tanaka, "A new method of scattering-angle scanning for optical beating light scattering spectroscopy," *Rev. Sci. Instrum.*, vol. 73, no. 2, pp. 263–269, Feb. 2002.
[27] F. Chouza, B. Witschas, and O. Reitebuch, "Heterodyne high-spectral-resolution LiDAR," *Appl. Opt.*, vol. 56, no. 29, pp. 8121-8134, Oct. 2017.
[28] Y. Minami, T. Yogi, and K. Sakai, "Rotational relaxation in H_2 gas observed with optical beating Brillouin spectroscopy," *J. Appl. Phys.*, vol. 106, no. 11, Dec. 2009, Art. no. 113519.
[29] T. Sonehara and H. Tanaka, "Forced Brillouin spectroscopy using frequency-tunable continuous wave lasers," *Phys. Rev. Lett.*, vol. 75, no. 23, pp. 4234–4237, Dec. 1995.
[30] T. Sonehara and H. Tanaka, "Forced Brillouin spectroscopy using optical generation of phonons," *Phys. B, Condens. Matter*, vols. 219–220, pp. 544–546, Apr. 1996.
[31] H. Tanaka and T. Sonehara, "Superheterodyne Brillouin spectroscopy using frequency-tunable lasers," *Phys. B, Condens. Matter*, vols. 219–220, pp. 556–558, Apr. 1996.
[32] A. Delahaigue, D. Courtois, C. Thiebeaux, S. Kalite, and B. Parvitte, "Atmospheric laser heterodyne detection," *Infr. Phys. Technol.*, vol. 37, no. 1, pp. 7–12, 1996.
[33] R. Kowarsch, R. Te, and C. Rembe, "Laser-Doppler vibrometer microscope with variable heterodyne carrier," *J. Phys., Conf. Ser.*, vol. 1149, Dec. 2018, Art. no. 012016.
[34] R. Kowarsch and C. Rembe, "Laser-Doppler vibrometry with variable GHz heterodyne carrier via frequency-offset lock," *Proc. SPIE*, vol. 10749, Aug. 2018, Art. no. 107490A.
[35] O. E. DeLange, "Optical heterodyne detection," *IEEE Spectr.*, vol. 5, no. 10, pp. 77–85, Oct. 1968.
[36] L. Mandel and E. Wolf, "Optimum conditions for heterodyne detection of light," *J. Opt. Soc. Amer.*, vol. 65, no. 4, p. 413, Apr. 1975.
[37] M. Teich, "Multiphoton optical heterodyne detection," *IEEE J. Quantum Electron.*, vol. QE-11, no. 8, pp. 595–602, Aug. 1975.
[38] C. Davis, "Single-photon optical heterodyning," *IEEE J. Quantum Electron.*, vol. QE-15, no. 1, pp. 26–29, Jan. 1979.
[39] H. P. Yuen and V. W. S. Chan, "Noise in homodyne and heterodyne detection," *Opt. Lett.*, vol. 8, no. 3, pp. 177–179, Mar. 1983.
[40] P. Campagne-Ibarcq, P. Six, L. Bretheau, A. Sarlette, M. Mirrahimi, P. Rouchon, and B. Huard, "Observing quantum state diffusion by heterodyne detection of fluorescence," *Phys. Rev. X*, vol. 6, no. 1, Jan. 2016, Art. no. 011002.
[41] C. Croal, C. Peuntinger, B. Heim, I. Khan, C. Marquardt, G. Leuchs, P. Wallden, E. Andersson, and N. Korolkova, "Free-space quantum signatures using heterodyne measurements," *Phys. Rev. Lett.*, vol. 117, no. 10, Sep. 2016, Art. no. 100503.
[42] H. Fearn and R. Loudon, "Quantum theory of the lossless beam splitter," *Opt. Commun.*, vol. 64, no. 6, pp. 485–490, Dec. 1987.
[43] M. J. Weber, *Handbook of Optical Materials*, 10th ed. Boca Raton, FL, USA: CRC Press, 2003.
[44] Y. Nishi, K. Mireskandari, P. Khaw, and O. Findl, "Lens refilling to restore accommodation," *J. Cataract Refractive Surg.*, vol. 35, no. 2, pp. 374–382, Feb. 2009.
[45] P. Benassi, V. Mazzacurati, G. Monaco, G. Ruocco, and G. Signorelli, "Brillouin and Raman cross sections in silicate glasses," *Phys. Rev. B, Condens. Matter*, vol. 52, no. 2, pp. 976–981, Jul. 1995.

MELANIE SCHÜNEMANN was born in Parchim, Germany, in 1988. She received the B.Sc., M.Sc., and Ph.D. degrees in physics from the University of Rostock, Rostock, Germany, in 2010, 2012, and 2018, respectively.

She is currently working with the Department of Ophthalmology, Rostock University Medical Center, Rostock, where she works on the application of quantum technologies in Brillouin spectroscopy. During her Ph.D. studies, she was a Visiting Researcher with the Department of Quantum Science, Australian National University, Canberra, Australia, and the JILA, University of Colorado, Boulder, USA. Her research interests include quantum optics and technologies and their application in life sciences.

Dr. Schünemann is a member of the Deutsche Physikalische Gesellschaft.

KARSTEN SPERLICH received the Ph.D. degree in physics from the University of Rostock, Germany, in 2017.

He was a Visiting Researcher with the Liquid Crystal Institute, Kent, OH, USA, in 2006. He currently works with the Department of Ophthalmology, Rostock University Medical Center, Rostock, Germany. His research interests include biomedical and biomechanical imaging, ultra-fast laser pulses, laser-tissue interaction, and their relation to ophthalmology.

Dr. Sperlich is a member of the Deutsche Physikalische Gesellschaft, the Deutsche Ophthalmologische Gesellschaft, and the Association for Research in Vision and Ophthalmology.

KAI BARNSCHEIDT received the B.Sc. and M.Sc. degrees in physics from the University of Rostock, where he is currently pursuing the Ph.D. degree in physics.

His research interests include the detection of short KERR-squeezed pulses and homodyne measurements of non-classicality and spectral quantum correlations. An additional special interest of his is the application of quantum optical measurement techniques to enhance biological imaging and nonlinear microscopy techniques beyond the limitations of classical optical using quantum correlations.

SAMUEL SCHÖPA received the B.Sc. and M.Sc. degrees in physics from the University of Rostock, Rostock, Germany, in 2019 and 2021, respectively. He is currently pursuing the Ph.D. degree in physics.

His research interest includes the application of machine learning in quantum optics.

JOHANNES WENZEL was born in Neustadt am Rübenberge, Hannover, Germany, in 1991. He received the B.Sc. and M.Sc. degrees in physics from the Leibniz University of Hannover, in 2019. He is currently pursuing the Ph.D. degree in physics with the Institute of Quantum Optics, Hannover. From 2014 to 2017, he was a Student Research Assistant at Rowiak GmbH. His research interests include the interaction of tissue with laser light and measurement techniques for rheological properties.

STEFAN KALIES studied physics at Leibniz University Hannover, Germany. He received the Ph.D. degree in the regenerative sciences program from the Hannover Medical School, Germany, in 2016. He is currently a Postdoctoral Researcher with the Institute of Quantum Optics, Leibniz University Hannover, and the Group Leader with the Lower Saxony Centre for Biomedical Engineering, Implant Research and Development. His research interests include the study of cell repair and tissue regeneration using imaging techniques and laser-based manipulation.

ALEXANDER HEISTERKAMP received the Ph.D. degree in physics. He is currently an Expert in biomedical optics, with a special interest in nonlinear imaging and manipulation of cells and tissues, laser therapy and diagnostics, and nanoparticle-laser interaction. He holds a Professorship in biophotonics at Leibniz University Hannover, Germany. Formerly, he was a Professor in physics at Friedrich-Schiller-University in Jena and he worked as the Department Head of the Laser Zentrum Hannover, both in Germany. He was a Postdoctoral Researcher with the Eric Mazur's Group, Harvard University, USA. He is a member of various societies and a fellow of SPIE.

HEINRICH STOLZ received the Ph.D. degree from the University of Paderborn, Paderborn, Germany, in 1979. He was a Researcher with the University of Paderborn, until 1996. Then, he joined the Faculty of Mathematics and Natural Science, University of Rostock, Rostock, Germany, and became the Chair of Semiconductor Physics, from which he retired, in 2015. His research interests include the field of semiconductor optics and especially in all aspects of exciton physics, including Rydberg excitons, ultrafast studies, and quantum optics. Furthermore, he is interested in the application of methods of semiconductor spectroscopy to other fields, such as biological systems.

OLIVER STACHS received the Ph.D. degree in physics from the University of Rostock, Rostock, Germany, in 1996, followed by a Leopoldina Fellowship for a visiting of the Stanford Synchrotron Radiation Laboratory, Stanford University, USA. In 2012, he was appointed as an Associate Professor in experimental ophthalmology with the University of Rostock, where he is currently the Scientific Group Leader of the experimental ophthalmology with the Department of Ophthalmology, University Medical Center. His research interests include the field of biomedical optics, ultra-high-field MRI, and the development of ophthalmic implants.

BORIS HAGE received the Ph.D. degree in physics from the Leibniz University of Hanover, Germany, in 2010. He spent two years with the Quantum Optics Group, Australian National University, as a Feodor-Lynen Fellow. In 2012, he was appointed as a Professor in experimental quantum optics with the University of Rostock, Germany. His research interests include centered around quantum metrology and quantum communication based on squeezed and entangled states of light.